Available online at www.sciencedirect.com
ScienceDirect
International Journal of Thermal Sciences 46 (2007) 682–691
International Journal of Thermal Sciences
www.elsevier.com/locate/ijts

Understanding heat transfer in 2D channel flows including recirculation

M.H. Dirkse [a,*], W.K.P. van Loon [a], J.D. Stigter [a], G.P.A. Bot [b]

[a] *Wageningen University, Bornsesteeg 59, 6708 PD Wageningen, The Netherlands*
[b] *Plant Research International, Bornsesteeg 65/16, 6700 AA Wageningen, The Netherlands*

Received 6 July 2006; received in revised form 29 August 2006; accepted 14 September 2006

Available online 23 October 2006

Abstract

Inviscid, irrotational two-dimensional flows can be modelled using the Schwarz–Christoffel integral. Although bounded flows including boundary layer separation and recirculation are not irrotational, a model is presented that uses the Schwarz–Christoffel integral to model these flows. The model separates the flow domain in the main flow area, where irrotational flow is assumed, and recirculation areas, which are modelled as monopolar vortices. The model has unknown parameters, which are geometric characteristics of the velocity field. The method is demonstrated on a channel with alternating baffles. Many variations of this system were modelled using CFD modelling, and the flow was a typical combination of main flow and recirculation. The CFD results were used as reference to calibrate the parameters of the Schwarz–Christoffel model. Many parameters appeared to be constant, and calibrating only three variable parameters yielded about 22% error for most velocity fields. After this, heat transfer was added to the CFD models, and the heat flux was analysed using the three variable parameters representing the velocity field. This way, a new model is found for the heat flux from a wall bounding a vortex, which has an error of 7%. Finally, we have calibrated the parameters using a limited number of given velocity vectors, demonstrating that the parameters can be calibrated against a real set of measurements.
© 2006 Elsevier Masson SAS. All rights reserved.

Keywords: Turbulent flow; Geometric transformation; Model reduction; Schwarz–Christoffel transformation; Computational fluid dynamics

1. Introduction

In many engineering problems, the heat flux by convection is of key importance. Given the temperature difference, the heat flux depends on the spatial distribution of velocity and fluid properties. Before the development of digital computers, the heat flux was calculated analytically, based on the most simple approximation of the velocity field: the average velocity [1,2]. Dimensionless power-law relations are applied in many engineering models. Complicated analytical derivations based on many assumptions are needed to find lumped models [1,3–5], so lumped models apply to specific systems only.

Two-dimensional flows can be modelled by assuming the flow to be inviscid and irrotational [3,6–8]. Given these assumptions, the velocity field can be calculated using conformal maps. These conformal maps can be calculated using the Schwarz–Christoffel integral [3]. The necessary calculations have been implemented in software libraries that calculate an entire velocity field within seconds [9,10]. In an earlier publication [11], we have extended these models to include boundary layer separation and flow recirculation driven by turbulent diffusion. Like any model some unknown parameters have to be calibrated against observations.

Currently, engineers use computational fluid dynamics (CFD) [12,13] to model the heat flux in complicated configurations. Commercial software packages that include the mathematical details are available. The scientific community has established concepts [14] and practices [15–17] to support reliable modelling. Due to these developments, CFD modelling is relatively easy nowadays, especially if two-dimensional models are applied. During design, many variations of a configuration can be modelled to evaluate their performance. However, computational fluid dynamics models give much more information than required for engineering decisions. Secondly, CFD models are too slow to be used as parts of larger engineering models [18]; and much too slow for implementation in automatic con-

* Corresponding author. Tel.: +31 317 483557; fax: +31 317 484957.
E-mail address: martijn.dirkse@wur.nl (M.H. Dirkse).

1290-0729/$ – see front matter © 2006 Elsevier Masson SAS. All rights reserved.
doi:10.1016/j.ijthermalsci.2006.09.004

Nomenclature

B	Baffle width	m
H	Length of flat plate or vertical baffle distance	m
Nu	Nusselt number	
P	Denotes a point in two-dimensional space	
Pr	Prandtl number	
Q	Denotes a point in two-dimensional space	
R	Radius of circular vortex	m
Re	Reynolds number	
V	Average inflow velocity	$\mathrm{m\,s^{-1}}$
$\dot{V}$	Two-dimensional volumetric flow rate	$\mathrm{m^2\,s^{-1}}$
W	Channel width	m
a	Real part of complex derivative of map g	$\mathrm{m^{-1}}$
b	Imaginary part of complex derivative of map g	$\mathrm{m^{-1}}$
g	Conformal map from physical space to unit disc	
i	Square root of -1	
k	Turbulent kinetic energy	$\mathrm{m^2\,s^{-2}}$
p	Parameter of regression line	
r	Distance from centre in circular vortex	m
u	Horizontal velocity	$\mathrm{m\,s^{-1}}$
u_∞	Velocity according to irrotational flow theory	$\mathrm{m\,s^{-1}}$
v	Vertical velocity	$\mathrm{m\,s^{-1}}$
x	Horizontal coordinate	m
y	Vertical coordinate	m

Greek symbols

ΔT	Temperature difference	K
Φ	Two-dimensional heat flux	$\mathrm{W\,m^{-1}}$
γ	Ellipticity	
η	Vertical coordinate on unit disc	
λ	Thermal conductivity of air	$\mathrm{W\,m^{-1}\,K^{-1}}$
ν	Kinematic viscosity	$\mathrm{m^2\,s^{-1}}$
ξ	Horizontal coordinate on unit disc	
ϕ	Potential function	$\mathrm{m^2\,s^{-1}}$
ψ	Stream function	$\mathrm{m^2\,s^{-1}}$
ω	Dissipation of turbulent kinetic energy	$\mathrm{s^{-1}}$

Superscripts

(main)	Main flow
(r)	Recirculation
(s)	Separation
(wake)	Wake

trollers. These two aspects demonstrate a need for simple tools to analyse flow phenomena.

This article focusses on turbulent two-dimensional flows including flow recirculation, with our earlier publication [11] on this subject as the starting point. The Schwarz–Christoffel model has unknown parameters, which are actually geometric characteristics of the velocity field. These characteristics describe the flow field as a combination of channel flow and recirculation wakes. We investigate whether this description is accurate, and whether the characteristics are useful for further model development. To do this, the Schwarz–Christoffel model is calibrated against known velocity fields. The parameters (geometric characteristics) are included in lumped models for the heat flux. It is examined (a) whether these models are accurate; (b) whether these models outperform conventional Nusselt–Reynolds correlations; and (c) whether the Schwarz–Christoffel model can be calibrated against real velocity measurements. The method is demonstrated for channel flow with baffles as an example for main flow and recirculation combination.

2. Theory

2.1. Irrotational flow

Since many technically important fluids have low viscosities (e.g. air or water), the majority of flows in practice are flows with high Reynolds number [4]. For these cases, viscous forces can be neglected compared to inertial forces nearly all over the flow field [3]. If the flow is also irrotational [3], it can be modelled by introducing the potential function ϕ ($\mathrm{m^2\,s^{-1}}$) and the stream function ψ ($\mathrm{m^2\,s^{-1}}$) [3]. When u and v are the components of the 2D velocity vector ($\mathrm{m\,s^{-1}}$), the potential function is defined to have $(u, v)'$ as its gradient; and the gradient of the stream function is defined to be $(-v, u)'$ [3]. When P and Q are two arbitrary locations in two-dimensional space, the difference $\psi(P) - \psi(Q)$ is the 2D volumetric flow rate ($\mathrm{m^2\,s^{-1}}$) through any curve joining P and Q [3]. The assumption of inviscid and irrotational flow makes the complex potential, defined as $\phi + i\psi$, an analytic function of space [3].

The complex potential can be used to calculate the entire velocity field in bounded infinite channels. The model inputs are the channel geometry and the 2D volumetric flow rate $\dot{V}$ ($\mathrm{m^2\,s^{-1}}$). By mass conservation, the stream function ψ is constant on both channel walls: $\psi = 0$ on one wall, $\psi = \dot{V}$ on the other. These conditions suffice to define a unique solution for the complex potential, which is calculated by mapping the channel onto the infinite strip. If the channel has a polygonal shape, the calculation can be performed using the Schwarz–Christoffel integral [3]. Software libraries have become available that evaluate the Schwarz–Christoffel integral numerically [9,10]. Driscoll [9] has programmed such a library for MatLab [19].

The velocity calculated by irrotational flow theory can be used to model the heat flux [5]. The following Nusselt–Reynolds correlation applies to turbulent flow past a flat plate if it is heated from the start, and if the velocity according to irrotational flow theory u_∞ ($\mathrm{m\,s^{-1}}$) is constant [5,20]:

$$Nu = \frac{\Phi}{\lambda \Delta T} = 0.0359 Pr^{0.6} \left(\frac{H u_\infty}{\nu} \right)^{0.8} \tag{1}$$

with: Φ the 2D heat flux ($\mathrm{W\,m^{-1}}$), λ the thermal conductivity ($\mathrm{W\,m^{-1}\,K^{-1}}$), ΔT the temperature difference (K), Pr the Prandtl number, H the length of the plate (m), and ν the kinematic viscosity $\mathrm{m^2\,s^{-1}}$.

2.2. Recirculation flow

The velocity field as calculated by irrotational flow theory does not satisfy the no-slip boundary condition. Indeed, thin areas with high velocity gradients are formed near solid walls, called boundary layers, where viscous effects are important. In some cases, a boundary layer separates from the wall where it is formed [3–5,21]. At the separation point, small vortices are convected into the bulk flow [3], which form a thin layer if the Reynolds number is high. This layer is called a vortex sheet [3, 22]. If the area behind the vortex sheet is bounded, turbulent momentum transport [4] through the vortex sheet causes recirculation flow.

Many researchers have proposed models for unbounded two-dimensional vortices [3,22–24]. A common model for monopolar unbounded vortices [24], Rankine's model, defines the velocity field via the stream function ψ [3]:

$$\psi = \psi^{(\mathrm{r})}\left(1 - \frac{r^2}{R^2}\right) \tag{2}$$

where $\psi^{(\mathrm{r})}$ is the 2D recirculation flow rate ($\mathrm{m^2\,s^{-1}}$); R is the fixed radius of the vortex (m); and r is the variable distance from the vortex centre (m). The velocity follows from differentiating Eq. (2).

Our earlier publication [11] develops a model for bounded two-dimensional vortices, which is part of the Schwarz–Christoffel model. As to our knowledge, we are the first to propose this model for bounded vortices. The model is inspired by Rankine's vortex model (Eq. (2)). Using the Schwarz–Christoffel integral, the vortex is mapped to the unit disc having coordinates ξ and η. The boundary of the vortex has become a circle, which allows us to introduce an equation for the stream function:

$$\psi = \psi^{(\mathrm{r})}\left(1 - \xi^2 - \eta^2\right) \tag{3}$$

This equation introduces the recirculation flow rate $\psi^{(\mathrm{r})}$ ($\mathrm{m^2\,s^{-1}}$) as a parameter. Given the map to the unit disc, Eq. (3) defines the stream function everywhere in the vortex; and the velocity field can be evaluated by differentiating Eq. (3).

Now, the map from the vortex to the unit disc must be specified. We start from the following assumptions: (a) the boundary of the vortex can be approximated by a polygon; and (b) the streamlines near the vortex centre look like ellipses. Furthermore, the model is applied to elongated vortex areas. For this reason, we have assumed also that: (c) the main axis of the ellipses of the recirculation is parallel to the vertical axis y. Assumption (b) does not specify the eccentricity of the ellipses (x-axis/y-axis). This eccentricity is introduced as a second parameter, $\gamma^{(\mathrm{r})}$.

To map a given location to the unit disc, we first multiply the vertical coordinate with the eccentricity. According to the assumptions, this transforms the elliptical streamlines into circles. A conformal map is applied to map these circular streamlines to the unit disc. Conformal maps are analytic complex functions [3,25], so the required map g can be evaluated using the Schwarz–Christoffel integral [9,10]. To define g uniquely, the coordinates of the vortex center must be introduced as parameters [9]: $x^{(\mathrm{r})}$ and $y^{(\mathrm{r})}$ (m).

The above is summarised by the equation $(\xi, \eta) = g(x, \gamma^{(\mathrm{r})} y)$. Combining this with Eq. (3) and differentiating yields:

$$\left(\frac{\partial\psi}{\partial x}, \frac{\partial\psi}{\partial y}\right) = (-v, u) = \psi^{(\mathrm{r})}(-2\xi - 2\eta)\begin{pmatrix} a & -b \\ b & a \end{pmatrix}\begin{pmatrix} 1 & 0 \\ 0 & \gamma^{(\mathrm{r})} \end{pmatrix} \tag{4}$$

where $a + bi$ is the complex derivative of g; a and b are in $\mathrm{m^{-1}}$. The model has four unknown parameters: the 2D recirculation flow rate $\psi^{(\mathrm{r})}$, the coordinates of the vortex centre ($x^{(\mathrm{r})}$, $y^{(\mathrm{r})}$), and the eccentricity $\gamma^{(\mathrm{r})}$. These four parameters are geometric characteristics, so four geometric characteristics can describe a monopolar vortex with a given boundary.

3. Materials and methods

3.1. Modelling the velocity field

The Schwarz–Christoffel model in general calculates the velocity field from the volumetric flow rate $\dot{V}$ and the shape of the flow domain. For this article, we considered a typical main flow and recirculation combination: consecutive chambers of a vertical channel including alternating baffles (Fig. 1), with the chamber defined as the area enclosed by two baffles. The design parameters are: vertical baffle distance H (m); channel width W (m); and baffle width B (m). All channels examined were variations of the default defined by $H = 1.00$ m, $W = 0.40$ m, $B = 0.20$ m (Table 1, row 1). The channels contained air flowing from the bottom to the top, and for every channel the following values for the average inflow velocity V ($\mathrm{m\,s^{-1}}$) were examined: 1.0, 2.0, 5.0, 10.0 and 25 $\mathrm{m\,s^{-1}}$. These design parameters were chosen to make the flow turbulent [1]: the Reynolds number VH/ν (ν is kinematic viscosity of air, $\mathrm{m^2\,s^{-1}}$) ranged from 6.8×10^3 to 3.4×10^6.

The Schwarz–Christoffel model had to be calibrated against given velocity fields, in this case generated by computational fluid dynamics (CFD) modelling. Six geometries (Table 1) and five velocities were modelled, resulting in 30 cases. The CFD cases were very similar to the one used in [11]. The velocity

Table 1
Design parameters H, W and B (Fig. 1) of the examined channels

Channel design number (–)	Vertical baffle distance H (m)	Channel width W (m)	Baffle width B (m)
1	1.00	0.400	0.200
2	1.50	0.400	0.200
3	2.00	0.400	0.200
4	1.00	0.400	0.100
5	1.00	0.400	0.150
6	0.10	0.040	0.020

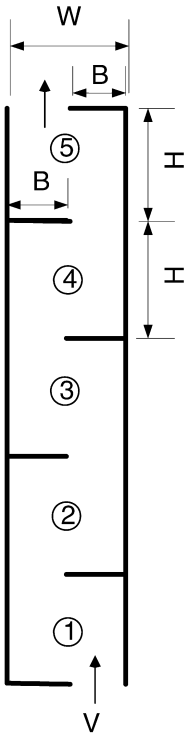

Fig. 1. Modelled configurations with design parameters H (m), W (m) and B (m); and with average inflow velocity V (m s^{-1}); the chambers are numbered.

and the pressure were solved from the incompressible steady Navier–Stokes equations [3], and the density and the viscosity of air were assumed to be temperature independent. The velocity was assumed to be uniform at the inflow opening at the bottom. The no-slip boundary condition was applied for the walls, and an outflow boundary condition at the top. The equations were solved using the commercial code Fluent [26].

The CFD cases used the k–ω turbulence model [13]. The boundary condition at the bottom for k and ω was expressed via the turbulence intensity [5,11,26]: the time-averaged magnitude of the fluctuating velocity [13] relative to the average inflow velocity V. The turbulence intensity at the bottom was set to 10%. A rectangular grid was used, which was generated using the commercial code Gambit [27]. To resolve the boundary layers, the grid intervals perpendicular to the channel walls had to be very small: 10^{-5} m. Dynamic grid adaption was applied to resolve the vortex sheets [17], and multiple refinement levels were compared to verify grid convergence [14,17].

The CFD velocity fields were calculated in a channel as depicted in Fig. 1, and the chambers in a channel were examined separately. Chamber number 1 and chamber number 5 (Fig. 1) were discarded, because the boundary conditions were very crude: parallel inflow at the bottom and an outflow boundary condition at the top. Therefore, each of the 30 CFD cases produced the velocity field in 3 chambers, resulting in 90 realisations of the velocity field. A realisation can be identified by the vertical baffle distance H, the channel width W, the baffle width B, the average inflow velocity V, and the chamber number (Fig. 1).

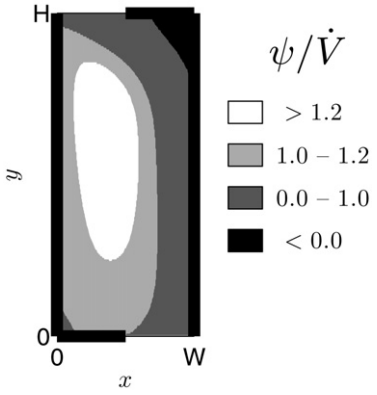

Fig. 2. Contour plot of stream function ψ (m^2 s^{-1}), calculated using computational fluid dynamics modelling; $\dot{V}$ is 2D volumetric air flow rate (m^2 s^{-1}); copied from [11].

A realisation of the velocity field constituted local velocities in tens of thousands of mesh cells, so this data was transformed to make it useful for calibration. The velocity field was truncated using a grid of 30 × 30 regularly arranged locations. For every location, the mesh cell closest to the location was selected, reducing the number of velocity vectors to 900. Fig. 1 shows that the even numbered chambers were reflected compared to the odd numbered chambers. When the realisation had an even chamber number, it was reflected by a coordinate transformation that replaced the x-coordinate with $W - x$. The result of these two transformations is called a calibration set, so there was one calibration set for each of the 90 realisations.

Since 900 local velocities cannot be measured, a virtual measurement set was derived from a calibration set. The virtual measurement set was based on 3 × 3 regularly arranged locations. For every location, the nearest velocity vector in the calibration set was selected. To save calculation time, virtual measurement sets were created only for the 15 (3 chamber numbers times 5 average inflow velocities) realisations corresponding to the default channel geometry (Table 1, number 1).

In previous research, the stream function has been calculated using CFD modelling, see Fig. 2. By definition of stream function (Section 2.1) and by mass conservation, the stream function on the main flow area must range from 0 to $\dot{V}$. The areas with stream function values outside this range must therefore correspond to recirculation areas. These areas are located at the top right and towards the left. The lines $\psi = 0$ and $\psi = \dot{V}$ correspond to areas of high vorticity (not shown). This observation confirms that separated boundary layers give rise to vortex sheets.

The Schwarz–Christoffel model approximates the vortex sheets by straight line segments, introducing vertices in the model of which the coordinates are parameters (free separation vertices) (Fig. 3). The chamber is extended to infinity by vertical line segments (Fig. 3). Irrotational flow is assumed over the area between the approximated streamlines $\psi = 0$ and $\psi = \dot{V}$, so this area is modelled by mapping it to the infinite strip (Section 2.1). The wake is modelled as a monopolar vortex using Eq. (4), and the top-right recirculation area is modelled to have zero velocity.

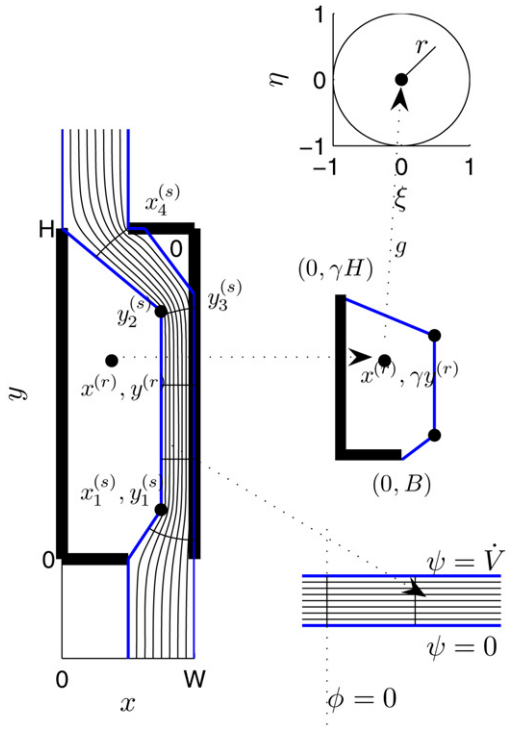

Fig. 3. Illustration of Schwarz–Christoffel model and its parameters.

Now, symbols are introduced for all parameters that characterise a velocity field (Fig. 3). The first separation vertex at the left vortex sheet is named $(x_1^{(s)}, y_1^{(s)})$. The y-coordinate of the second separation vertex to the left is named $y_2^{(s)}$ and its x-coordinate is always taken to be $x_1^{(s)}$ to minimise the number of parameters. The coordinates describing the right vortex sheet are named $y_3^{(s)}$ and $x_4^{(s)}$. The four parameters describing the wake are the coordinates of the vortex centre $(x^{(r)}, y^{(r)})$, the recirculation flow rate $\psi^{(r)}$, and the eccentricity $\gamma^{(r)}$.

The algorithm that calculates the model parameters starts from a given calibration set or virtual measurement set. Parameter values are optimised such that minimisation of the difference between the velocity field according to the Schwarz–Christoffel model, and the velocity field in the calibration set, i.e. the global velocity error, is achieved. The global velocity error is the root-mean-square of the local velocity errors at the locations in the calibration set. The local velocity error is the norm of the vector that contains the error of the horizontal velocity and the error of the vertical velocity. The Schwarz–Christoffel integral has singularities at vertices having an internal angle of more than 180° (e.g. $(x_1^{(s)}, y_1^{(s)})$ in Fig. 3), so it makes no sense to observe the local velocity error there. The global velocity error is iteratively minimised by Sequential Quadratic Programming (SQP) [28]. Ten different random initialisations are applied and the parameter values corresponding to the lowest velocity error are selected. The ten runs of SQP can be compared to obtain error estimates for each parameter separately.

To examine the relevance of each model parameter, calibration was performed using different subsets of the parameters. Leaving out $y_3^{(s)}$ and $x_4^{(s)}$, for example, implied that boundary layer separation at the top-right was not included in the model. All subsets were calibrated against the same calibration set, and the corresponding velocity errors were compared. Based on this comparison, we selected the parameters that were relevant to describe a velocity field. Different velocity fields generally correspond to different values of the parameters, so the relevant parameters were expected to be different for every calibration set.

The selected parameters were calculated for all realisations, resulting in 90 realisations for every parameter. Each parameter was made dimensionless and its mean and variation (root-mean-square of deviations from the mean) were calculated. A parameter was assumed constant if its variation was low compared to the accuracy of the calibration algorithm, allowing for a reduction of the number of parameters needed. The variable parameters were recalculated to test the impact of making parameters constant.

To analyse the variable parameters, the modelled realisations were divided into six groups that corresponded to the six channel geometries (Table 1). Each modelled geometry constituted 15 realisations, which corresponded to 15 realisations of each variable parameter. The mean of a parameter over these realisations is referred to as a geometry mean. The impact of velocity and chamber number on a parameter was assessed using its range (over 15 parameter realisations).

The variable parameters were also calibrated against the virtual measurement sets to examine whether these parameters can be measured. The virtual measurements of the parameters were analysed by relating them to the parameter realisations obtained using the large calibration sets, the calibrated values. For every variable parameter, a linear regression model was created that explained the 15 (only one modelled geometry) virtual measurements from the calibrated values. The R^2-value of the regression, the percentage of variance explained by the regression model, was used as a measure for the agreement of the virtual measurements.

3.2. Lumped models for heat transfer

The main objective of this paper is modelling heat transfer, so the CFD models of Section 3.1 were extended to include heat transfer. The channel walls were modelled to have a constant temperature, which was 10 K higher than the temperature of the incoming air. Buoyancy effects could be neglected for the chosen design parameters [3], so it was only needed to solve the energy equation extra to the existing solution of the Navier–Stokes equations. The heat fluxes from the two walls of every chamber (Fig. 1) were considered separately, because Eq. (1) is valid for the heat flux from the wall next to the main flow area ($\Phi^{(\text{main})}$, $\mathrm{W\,m^{-1}}$), but not for the wall next to the wake ($\Phi^{(\text{wake})}$).

The CFD $\Phi^{(\text{main})}$ and $\Phi^{(\text{wake})}$ were analysed taking into account that the air was heated in preceding chambers, so $\Delta T^{(\text{main})}$ was defined as the temperature difference between the chamber inflow and the walls. $\Phi^{(\text{wake})}$ was analysed using the conditions in the wake only, so $\Delta T^{(\text{wake})}$ was defined as the temperature difference between the wall and the vortex cen-

tre. Using these temperature differences, the following Nusselt numbers were defined:

$$Nu^{(\text{main})} = \frac{\Phi^{(\text{main})}}{\lambda \Delta T^{(\text{main})}}, \qquad Nu^{(\text{wake})} = \frac{\Phi^{(\text{wake})}}{\lambda \Delta T^{(\text{wake})}} \tag{5}$$

where λ is the thermal conductivity of air ($\mathrm{W\,m^{-1}\,K^{-1}}$).

Without information about the velocity field, a power law model for $Nu^{(\text{main})}$ is generally assumed:

$$Nu^{(\text{main})} = p_1 Re^{p_2} \tag{6}$$

$$Re = V\,H/\nu \tag{7}$$

where p_1 and p_2 are parameters to be determined by linear regression. The regression error could be transformed to a relative error for $Nu^{(\text{main})}$, because $\log Nu^{(\text{main})}$ was used to draw the regression line. The variable parameters of the Schwarz–Christoffel model were used to define modified Reynolds numbers, which were also used to model $Nu^{(\text{main})}$. In this way, the relevance of the Schwarz–Christoffel model parameters for the heat flux could be investigated. The same procedure was applied to model $Nu^{(\text{wake})}$: $Nu^{(\text{wake})}$ was first modelled using Re (Eq. (7)), and modified Reynolds numbers based on the Schwarz–Christoffel model parameters were used after that.

Finally, a power law model for the total heat flux $\Phi^{(\text{main})} + \Phi^{(\text{wake})}$ was created for reference. The total heat flux was modelled using the total Nusselt number defined by:

$$Nu^{(\text{tot})} = \frac{\Phi^{(\text{main})} + \Phi^{(\text{wake})}}{\lambda \Delta T^{(\text{main})}} \tag{8}$$

and $Nu^{(\text{tot})}$ was related to the standard Reynolds number Re.

4. Results and discussion

4.1. Selection of parameters

A velocity field calculated with CFD, as shown in Fig. 4(a), was used to calibrate the Schwarz–Christoffel model including different numbers of parameters. When no parameters were included, the Schwarz–Christoffel model mapped the entire flow domain to the strip. The velocity field was not modelled correctly in this case as demonstrated in Fig. 4(b). The root-mean-square of the local errors over the 900 locations in the calibration set was 88% relative to the average inflow velocity (Table 2, first line).

With one free separation vertex and a circular wake, five parameters were used, which resulted in a large reduction of the error to 42% (Table 2, third line). The most efficient way to add the sixth parameter was to introduce a second separation vertex (reduction to 32% error). Making the recirculation elliptic after this reduced the error by 4 to 28%, requiring seven para-

Table 2
Velocity errors resulting from different parameter selections relative to CFD model results; calibration for $H = 1.0$ m, $W = 0.40$ m, $B = 0.20$ m, $V = 5.0\ \mathrm{m\,s^{-1}}$, chamber number 3

Left vortex sheet	Right vortex sheet	Left num. sep. vertices	Left recirc. type	Number of parameters	Relative velocity error
no	no	–	–	0	88
yes	no	1	zero	2	58
yes	no	1	circular	5	42
yes	no	1	elliptic	6	40
yes	no	2	circular	6	32
yes	yes	1	circular	7	41
yes	no	2	elliptic	7	28
yes	yes	1	elliptic	8	38
yes	yes	2	elliptic	9	24

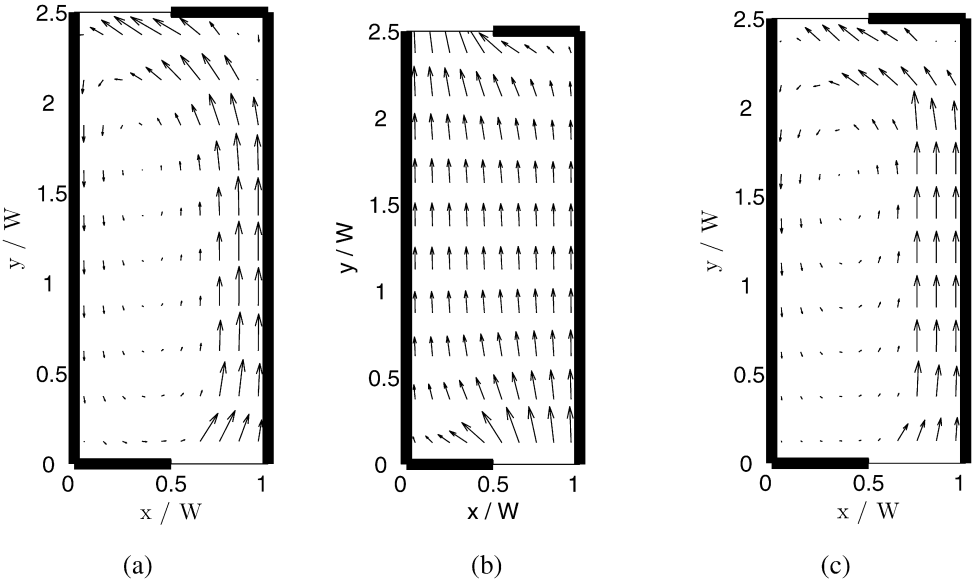

Fig. 4. Qualitative agreement between CFD model and Schwarz–Christoffel model for $H = 1.0$ m, $W = 0.40$ m, $B = 0.20$ m, $V = 5.0\ \mathrm{m\,s^{-1}}$ and chamber number 3; (a) CFD model; (b) Schwarz–Christoffel model without boundary layer separation (Table 2, first row); (c) Schwarz–Christoffel model using nine parameters (Table 2, last row).

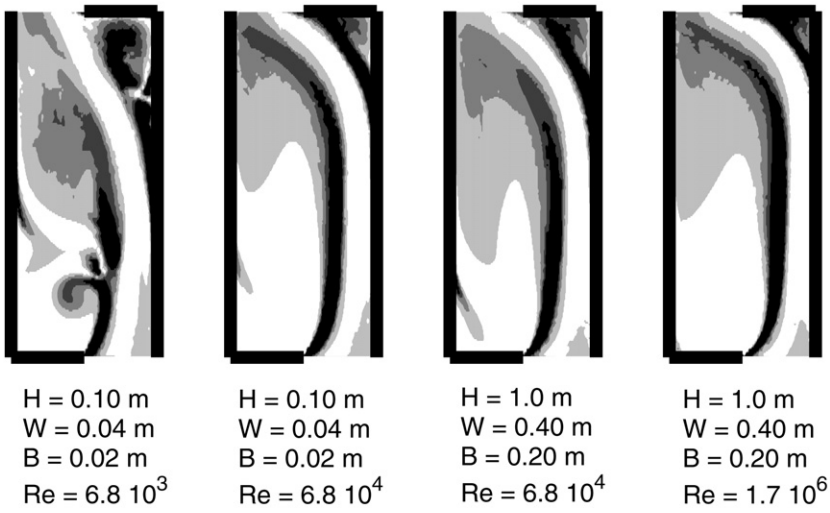

Fig. 5. CFD calculated contour plots of vorticity magnitude for different Reynolds numbers.

meters. This reduction verified the importance of the ellipticity parameter stated in [11]. When all parameters of Section 3.1, nine parameters, were used, the error was 24%. This parameter selection made the Schwarz–Christoffel model agree with the CFD model as shown in Fig. 4(c): large velocities on the right, smaller velocities on the left, recirculation behind the lower baffle and very small velocities at the lower-left corner.

The nine parameters were calibrated for a total of 90 realisations (6 channel geometries times 5 velocities times 3 chamber numbers: 2, 3 and 4, see Fig. 1). The velocity error of 24% listed in Table 2, was typical the velocity error calculated for all modelled realisations, because the average of these errors was 22% and their standard deviation was 4%. For each channel geometry, the velocity error increased for increasing chamber number (Fig. 1), and this effect was significant according to a t-test. This effect was related to an increase of the local velocities in the recirculation areas, making these areas more important compared to the main flow area. The velocity error was also high for low Reynolds numbers (geometry 6 of Table 1); up to 35% for chamber number 3 and average inflow velocity $V = 1.0\ \mathrm{m\,s^{-1}}$ (corresponding Reynolds number 6.8×10^3). This large velocity error was caused by deviating vorticity fields according to the CFD models, as demonstrated in Fig. 5. For instance the vorticity field for $Re = 6.8 \times 10^3$ deviates considerably from the vorticity fields for higher Reynolds numbers as can be seen in Fig. 5.

Over the 90 realisations, the standard deviation of the dimensionless parameter $y_1^{(s)}/H$ (see Fig. 3 for meaning of $y_1^{(s)}$) was 0.07. The error of the calibration algorithm for $y_1^{(s)}/H$, estimated using the ten runs of Sequential Quadratic Programming (Section 3.1), was 0.08. These numbers demonstrated that the variation of $y_1^{(s)}/H$ was fully explained by the error of the calibration algorithm. Therefore, $y_1^{(s)}/H$ was assumed constant, and the constant value was the mean over the 90 realisations: $y_1^{(s)}/H = 0.14$. The same applied for two other parameters, resulting in the constant values $y_3^{(s)}/H = 0.78$ and $y^{(r)}/H = 0.61$. Three additional parameters had part of their variation explained by the error of the calibration algorithm, and the following constant values were assumed: $\gamma^{(r)}H/B = 2.33$, $x_4^{(s)}/W = 0.77$ and $y_2^{(s)}/H = 0.73$. The remaining variable parameters were $x_1^{(s)}/W$, $x^{(r)}/W$ and $\psi^{(r)}/\dot{V}$. Their values were recalculated using the constant parameter values listed above, and this calculation was performed for every realisation.

Table 3
Statistics of variable parameters over default modelled geometry (15 realisations per parameter); geometry means and parameter domains (first three rows), and agreement of virtual measurements (last row)

	Relative wake width $x_1^{(s)}/W$	Relative wake centre $x^{(r)}/W$	Relative recirculation flow rate $\psi^{(r)}/\dot{V}$
Channel mean	0.71	0.37	0.34
Minimum	0.65	0.35	0.26
Maximum	0.77	0.40	0.42
Agreement virt. measurements (%)	95	69	81

Using three instead of nine parameters caused only a small increment of the relative velocity error. For the chamber of Fig. 4, the error remained 24% (Table 2, last row). The error increased only two percent averaged (root-mean-square) over the fifteen realisations having the default geometry (Table 1, number 1). The averaged error increments were below 4% for geometry numbers 2–5 of Table 1. The highest average increment, 5%, was found for low Reynolds numbers (Table 1, number 6), and this value is explained by deviating vorticity fields as calculated by CFD modelling (Fig. 5).

To analyse the values for the variable parameters, the 15 realisations corresponding to the default geometry are considered first. The geometry mean of $x_1^{(s)}/W$ was 0.71 (Table 3, first row), so the width of the wake was more than the baffle width B ($B/W = 0.5$, see Table 1). This number also demonstrated that the main flow was contracted. The geometry mean of $x^{(r)}/W$ was about half the mean of $x_1^{(s)}/W$ (Table 3, first row), which meant that the vortex centre was located in the horizontal middle of the wake. Vertically, the vortex centre was located towards the top, because the $y^{(r)}/H = 0.61$ constant

Table 4
Influence of geometry on Schwarz–Christoffel model parameters; + = positive correlation and − = negative correlation

Dimensionless model parameter	Design parameter		
	Chamber height H	Baffle width B	Reynolds number
Relative wake width $x_1^{(s)}/W$	−	+	+
Relative wake centre $x^{(r)}/W$	+	+	0[a]
Relative recirculation flow rate $\psi^{(r)}/\dot{V}$	−	+	+

[a] The difference between the relevant geometry means was not significant according to a t-test with significance level 5%.

parameter was more than 0.50. The ranges of the dimensionless parameters were small compared to the geometry means (Table 3, second and third row).

The channel geometries numbered 2 and 3 in Table 1 differed from the default channel geometry only by the vertical baffle distance H. The channel geometries numbered 4 and 5 differed only by the baffle width B, and geometry number 6 was scaled to model lower Reynolds numbers. The impact of geometry on the parameter values was analysed by comparing the geometry means for the different geometries with the default geometry. It appeared that increasing the baffle width widened the wake, increasing the flow rate in the wake as well (Table 4, second column). Increasing the vertical baffle distance H moved the vortex centre to the right and reduced the wake width and the flow rate in the wake (Table 4, first column). Increasing the Reynolds number widened the wake and increased the recirculation flow rate, but had no impact on the location of the vortex centre.

To examine whether the variable parameters can be measured, the calibration algorithm was applied on reduced calibration sets, called virtual measurement sets (3×3 regularly arranged velocity vectors). The virtual measurements of the parameters were analysed by comparing them with the parameter realisations obtained using the large calibration sets. The parameter $x^{(r)}/W$ could be measured the least accurate, because the agreement (R^2-value of the regression) was 69%. The parameters $\psi^{(r)}/\dot{V}$ and $x_1^{(s)}/W$ could be measured satisfactory (81%, respectively, 95% agreement).

4.2. Use of Schwarz–Christoffel parameters to model heat transfer

The Schwarz–Christoffel model parameters were used to model heat transfer. Fig. 6 shows a typical temperature field obtained by CFD modelling, for chamber number 3; the walls are 10 K warmer than the channel inflow temperature. There was a temperature increment of less than 1 K at the chamber inflow opening, because the air was heated in the two preceding chambers. The air temperature did not increase much in the main flow area, but the temperature was higher in the wake and in the recirculation area at the top-right. These higher temperature increments were explained by the longer contact times between the air and the walls there. The temperature in the wake was

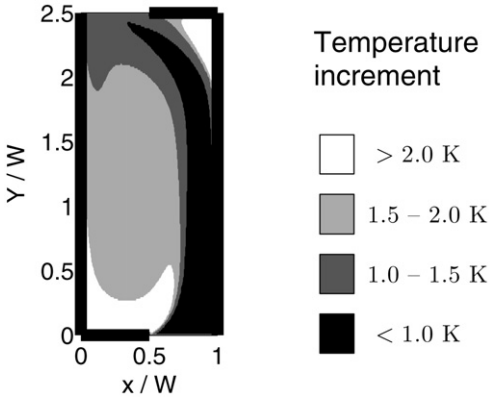

Fig. 6. Temperature field according to CFD model; $H = 1.0$ m, $W = 0.40$ m, $B = 0.20$ m, $V = 5.0$ m s^{-1}, chamber number 3; the channel walls are 10 K warmer than the channel inflow temperature.

Table 5
Nusselt–Reynolds correlations modelling the total heat flux, the main heat flux and the wake heat flux using relevant modified Reynolds numbers; H, W and B design parameters (Fig. 1), V is average inflow velocity, $\dot{V}$ is volumetric flow rate (m^2 s^{-1}), ν kinematic viscosity (m^2 s^{-1})

Seq. number	Side	Reynolds	Power-law (Eq. (6))		Relative error
			p_1	p_2	
1	total	HV/ν	0.041	0.80	17
2	main	HV/ν	0.043	0.81	22
3	main	$H\dot{V}/\nu(W - x_1^{(s)})$	0.041	0.79	11
4	wake	BV/ν	0.201	0.79	20
5	wake	HV/ν	0.075	0.75	12
6	wake	$(x^{(r)}/B)(HV/\nu)$	0.111	0.72	17
7	wake	$(x_1^{(s)}/B)(HV/\nu)$	0.072	0.73	15
8	wake	$(\psi^{(r)}/B)H/\nu$	0.214	0.73	12
9	wake	$H\psi^{(r)}/x^{(r)}\nu$	0.151	0.75	9
10	wake	$H\psi^{(r)}/x_1^{(s)}\nu$	0.225	0.75	7

rather homogeneous as well, justifying that a wake temperature was defined (Section 3.2). The 2D heat flux corresponding to Fig. 6 was 561 W m^{-1}, which was represented by a Nusselt number of 1250. The Nusselt numbers corresponding to all realisations ranged from 44 to 7900, and they could be modelled using the standard Reynolds number (Eq. (7)) with an error of 17% (Table 5, number 1).

Improved relations for the main and wake heat fluxes were found by analysing them separately (Section 3.2). The main flow area is described by $x_1^{(s)}$, $y^{(1)}$, $y^{(2)}$, $y_3^{(s)}$ and $x_4^{(s)}$ (Fig. 3). From this list, only $x_1^{(s)}$ is variable and hence is relevant to be included in modified Reynolds numbers. This parameter was used to model the width of the main flow, defining a new characteristic velocity. The characteristic length in the modified Reynolds number remained the chamber height H, keeping the analogy with a flat plate. The modified Reynolds number predicted $\Phi^{(\text{main})}$ better than the standard Reynolds number (Table 5, numbers 2 and 3): the error reduced from 22 to 11%.

The main heat flux was also modelled using the virtually measured values of $x_1^{(s)}$, obtained from calibration with the reduced calibration sets as reference. These parameter values

Table 6
Relative errors of regression models for the main heat flux and the wake heat flux, based on virtual measurements and calibrated parameter values; regression only over default modelled geometry (15 realisations)

1	main	–	HV/ν	17
2	main	calibrated	$H\dot{V}/\nu(W-x_1^{(s)})$	5.1
3	main	measured	$H\dot{V}/\nu(W-x_1^{(s)})$	5.8
4	wake	–	VH/ν	9
5	wake	calibrated	$H\psi^{(r)}/x_1^{(s)}\nu$	2.9
6	wake	measured	$H\psi^{(r)}/x_1^{(s)}\nu$	5.3

were only calculated for the default modelled channel. Using only the standard geometry instead of all geometries, the relative error for the standard Reynolds number reduced from 22% (Table 5) to 17% (Table 6, row 1). The modified Reynolds number, containing the wake width $x_1^{(s)}$, allowed the heat flux to be modelled much more accurately. Based on the virtual measurements, the error was only 5.8% (Table 6, row 3). Based on the parameter values obtained from the large calibration sets, the error was not much lower: 5.1% (Table 6, row 2). These results demonstrate that the main heat flux can also be calculated using parameter values obtained from a small number of measured velocities.

The wake heat flux was first modelled without model parameters. Using the baffle width B as the characteristic length yielded 20% error (Table 5, number 4), but using the vertical baffle distance H yielded 12% (Table 5, number 5). Secondly, one model parameter was included in the Reynolds number in such a way that the characteristic length remained the vertical baffle distance (Table 5, numbers 6–8). The best parameter to include appeared to be the recirculation flow rate $\psi^{(r)}$, resulting in an error of 12%. The corresponding Reynolds number was $(\psi^{(r)}/B)H/\nu$, so the area containing the recirculation flow was characterised by the baffle width. Finally, better Reynolds numbers were obtained by replacing the baffle width by the horizontal coordinate of the wake centre, or by the wake width (Table 5, numbers 9–10). The Reynolds number $(\psi^{(r)}/x_1^{(s)})H/\nu$ yielded 7% error, a dramatic improvement to the default Reynolds number VH/ν.

The wake heat flux was also modelled using the virtual measurements. For reference, the standard Reynolds number was used to model the wake heat flux for only the default channel geometry, yielding 9% error (Table 6, number 4). The best modified Reynolds number, $(\psi^{(r)}/x_1^{(s)})H/\nu$, as calculated using normal calibration, yielded 2.9% error (Table 6, number 5). When the virtual measurements were used instead, the error was still only 5.3% (Table 6, number 6). Therefore, the wake heat flux can be calculated using parameter values obtained from a small number of measured velocities.

5. Conclusions

The channel-baffle geometry is a good example to demonstrate main flow and recirculation combination. Based on the Schwarz–Christoffel transformation, a new model for these flows has been presented. It assumes irrotational flow in the main flow area, and the wake is modelled as a monopolar vortex. The Schwarz–Christoffel model needs nine parameters to be estimated, which are geometric characteristics of the velocity field: two vertical coordinates and one horizontal coordinate (wake width) defining straight line segments bounding the wake; the vertical coordinate of the separation point before a baffle; the horizontal coordinate of the corresponding reattachment point; the two coordinates of the vortex centre of the wake; the two-dimensional recirculation flow rate; and the ellipticity of the recirculation in the wake.

The parameters in the model were calibrated for different baffle distances H (m), channel widths W (m), baffle widths B, average inflow velocities V and chamber sequence numbers, corresponding to Reynolds numbers ranging from 6.8×10^3 to 3.4×10^6. Six parameters appeared to be constant in dimensionless form: the two vertical coordinates defining the wake boundary ($y_1^{(s)}/H = 0.14$ and $y_2^{(s)}/H = 0.73$); the vertical coordinate of the separation point before a baffle ($y_3^{(s)}/H = 0.78$); the horizontal coordinate of the corresponding reattachment point ($x_4^{(s)}/W = 0.77$); the vertical coordinate of the centre of the recirculation in the wake ($y^{(r)}/H = 0.61$); and the ellipticity of the recirculation ($\gamma^{(r)}H/B = 2.33$). The remaining variable parameters were the dimensionless wake width $x^{(s)}/W$, the dimensionless horizontal coordinate of the vortex centre $x^{(r)}/W$, and the dimensionless recirculation flow rate $\psi^{(r)}/\dot{V}$ where $\dot{V}$ is the two-dimensional volumetric flow rate in the main flow area, in $\mathrm{m^2\,s^{-1}}$. Calibrating only these three parameters, instead of nine, causes only a small increase of the velocity error. With three calibrated parameters, the velocity error becomes only about 23%. Higher velocity errors only occur for the lowest Reynolds numbers, which can be explained by the vorticity field (according to CFD modelling) being different.

According to CFD modelling results, a constant temperature on the channel walls does not cause a large temperature increase in a chamber, but the temperatures in both recirculation areas are higher than the temperature in the main flow area. The heat flux from the walls can be modelled with 17% error using a standard Nusselt–Reynolds correlation. The two walls of a chamber must be considered separately, however, because there are different flow regimes near both walls. These heat fluxes can be modelled more accurately using the three variable parameters. The heat flux into the main flow is modelled with 22% error using the standard Reynolds number, but a modified Reynolds based on the wake width, $Re^{(\mathrm{main})} = H\dot{V}/\nu(W - x_1^{(s)})$, yields 11% error ($\nu$ is kinematic viscosity in $\mathrm{m^2\,s^{-1}}$): the correlation reads $Nu^{(\mathrm{main})} = 0.041\,Re^{(\mathrm{main})^{0.79}}$ where $Nu^{(\mathrm{main})}$ is a Nusselt number expressing the heat flux into the main flow. The heat flux into the wake is modelled with 12% error using the standard Reynolds number, but 7% can be achieved with a modified Reynolds number including the recirculation flow rate and the wake width, $Re^{(\mathrm{wake})} = H\psi^{(r)}/x_1^{(s)}\nu$: the correlation reads $Nu^{(\mathrm{wake})} = 0.225\,Re^{(\mathrm{wake})^{0.75}}$ where $Nu^{(\mathrm{wake})}$ is a Nusselt number expressing the heat flux into the wake. This new power-law relation applies to bounded vortices in general, because the heat flux is modelled from only the conditions in the wake.

The parameter values can also be calculated using small calibration sets having nine velocity vectors only, which can be regarded as virtual measurements. The parameters obtained from nine virtual measurements are only slightly different from the values obtained using large calibration sets. For fixed channel geometry, the heat flux into the main flow can be modelled with 5.8% error using the wake width, to be compared with 17% error from the standard Reynolds number. The heat flux into the wake can be modelled with 5.3% error, to be compared with 9% error from the standard Reynolds number. These numbers show that the heat flux can be calculated accurately from a limited number of velocity measurements.

To summarise, the Schwarz–Christoffel model has been used successfully to model the examined channel-baffle geometry. The parameters are geometric characteristics and the velocity field corresponding to given parameter values can be evaluated quickly. In addition, the parameter values can be applied in power-law models for the heat flux. All calculations were carried out with air as the flowing medium, but the medium influences the heat flux only via the Prandtl number. The Prandtl number has a limited impact and it is known that all gasses have a Prandtl number near 1. Since the examined geometry is a typical combination of main flow and recirculation flow, we conclude that the Schwarz–Christoffel model is a useful tool to model two-dimensional turbulent flows of gasses.

References

[1] D.R. Gaskell, An Introduction to Transport Phenomena in Materials Engineering, Macmillan Publishing Company, New York, USA, 1992.

[2] R.H. Perry, D.W. Green, Perry's Chemical Engineering Handbook, seventh ed., McGraw–Hill, Singapore, 1997.

[3] G.K. Batchelor, An Introduction to Fluid Dynamics, Cambridge Univ. Press, Cambridge, UK, 1967.

[4] H. Schlichting, Boundary Layer Theory, Springer-Verlag, Berlin–Heidelberg, 2000.

[5] W.M. Kays, M.E. Crawford, Convective Heat and Mass Transfer, McGraw–Hill Series in Mechanical Engineering, McGraw–Hill, New York, 1993.

[6] L.M. Conroy, P.M.J. Trevelyan, D.B. Ingham, An analytical, numerical, and experimental comparison of the fluid velocity in the vicinity of an open tank with one and two lateral exhaust slot hoods and a uniform cross-draft, Ann. Occup. Hyg. 44 (6) (2000) 407–419.

[7] P.M.J. Trevelyan, L. Elliott, D.B. Ingham, Potential flow in a semi-infinite channel with multiple sub-channels using the Schwarz–Christoffel transformation, Comput. Methods Appl. Mech. Engrg. 189 (2000) 341–359.

[8] W.C. Hassenpflug, Branched channel free-streamlines, Comput. Methods Appl. Mech. Engrg. 159 (1998) 329–354.

[9] T.A. Driscoll, Algorithm 756: A MATLAB toolbox for Schwarz–Christoffel mapping, ACM Trans. Math. Software 22 (2) (1996) 168–186.

[10] L.N. Trefethen, T.A. Driscoll, Schwarz–Christoffel mapping in the computer era, Doc. Math. 3 (1998) 533–542 (extra volume ICM).

[11] M.H. Dirkse, W.K.P.V. Loon, J.D. Stigter, G.P.A. Bot, A simple model for obstructed two-dimensional turbulent channel flow, in: Numerical Heat Transfer (Eurotherm Seminar 82), Institute of Thermal Technology, Silesian University of Technology, Gliwice, Poland, 2005, pp. 983–992.

[12] S.V. Patankar, Numerical Heat Transfer and Fluid Flow, Series in Computational Methods in Mechanics and Thermal Sciences, Taylor & Francis, USA, 1980.

[13] D.C. Wilcox, Turbulence Modeling for CFD, DCW Industries, Inc., La Canada, CA, 1998.

[14] W.L. Oberkampf, T.G. Trucano, Verification and validation in computational fluid dynamics, Prog. Aerospace Sci. 38 (2002) 209–272.

[15] R.V. Wilson, F. Stern, H.W. Coleman, E.G. Paterson, Comprehensive approach to verification and validation of CFD simulations—part 2: Application for Rans simulation of a Cargo/Container ship, J. Fluids Engrg. 123 (4) (2001) 803–810.

[16] F. Stern, R.V. Wilson, H.W. Coleman, E.G. Paterson, Comprehensive approach to verification and validation of CFD simulations—part 1: Methodology and procedures, J. Fluids Engrg. 123 (4) (2001) 793–802.

[17] D. Lacasse, É. Turgeon, D. Pelletier, On the judicious use of the k–ϵ model, wall functions and adaptivity, Int. J. Thermal Sci. 43 (2004) 925–938.

[18] V.S. Gullapalli, F. Strömer, O. Pelletier, Component based performance analysis of compact brazed plate heat exchangers, in: Numerical Heat Transfer (Eurotherm Seminar 82), Institute of Thermal Technology, Silesian University of Technology, Gliwice, Poland, 2005, pp. 1015–1022.

[19] The Math Works, http://www.mathworks.com/, 2006.

[20] T.A. Ameel, Average effects of forced convection over a flat plate with an unheated starting length, Int. Commun. Heat Mass 24 (8) (1997) 1113–1120.

[21] H.I. Abu-Mulaweh, Turbulent mixed convection flow over a forward-facing step—the effect of step heights, Int. J. Thermal Sci. 44 (2005) 155–162.

[22] P.G. Saffman, Vortex Dynamics, Cambridge Monographs on Mechanics and Applied Mathematics, Cambridge Univ. Press, Cambridge, UK, 1992.

[23] A.R. Paterson, A First Course in Fluid Dynamics, Cambridge Univ. Press, Cambridge, UK, 1983.

[24] M.P. Satijn, M.G.V. Buren, H.J.H. Clercx, G.J.F.V. Heijst, Vortex models based on similarity solutions of the two-dimensional diffusion equation, Phys. Fluids 16 (11) (2004) 3997–4011.

[25] J.P. Keener, Principles of Applied Mathematics: Transformation and Approximation, Addison–Wesley Publishing Company, Reading, MA, 1988.

[26] Fluent Inc., Lebanon, USA, FLUENT 6.1 documentation, http://www.fluent.com, 2003.

[27] Fluent Inc., Lebanon, USA, GAMBIT 2.1 documentation, http://www.fluent.com, 2002.

[28] K. Schittowski, NLQPL: A FORTRAN-subroutine solving constrained nonlinear programming problems, Ann. Oper. Res. 5 (1985) 485–500.